Available online at www.sciencedirect.com
SCIENCE DIRECT®
Journal of Sound and Vibration 267 (2003) 523–535
JOURNAL OF SOUND AND VIBRATION
www.elsevier.com/locate/jsvi

The influence of the contact zone on the excitation of wheel/rail noise

D.J. Thompson*

Institute of Sound and Vibration Research, University of Southampton, Southampton SO17 1BJ, UK

Accepted 9 May 2003

Abstract

Rolling noise is excited by surface roughness at the wheel/rail contact. The contact patch is known to attenuate the excitation at wavelengths that are short in comparison with its length. A distributed point-reacting spring (DPRS) model is used with measured roughness data to determine the contact filter effect, and this result is compared with analytical predictions. It is found that the analytical model gives an attenuation that is too large at short wavelengths but is usable for wavelengths down to somewhat smaller than the length of the contact patch. Additionally, variations in the detailed geometry of the profile can cause the contact point on the wheel and rail to oscillate laterally. This introduces an oscillating moment that can induce additional vibration and noise. The DPRS model and rolling noise prediction model are both extended and used together to allow an estimate of the contribution to the radiated noise. It is found that, while the direct roughness excitation is still more important, the moment excitation can be significant, particularly for conforming profiles.

1. Introduction

Rolling noise is excited at the contact between wheel and rail by the roughness of their surfaces, which induces vibration in the form of a vertical relative displacement [1]. The contact zone has an influence on rolling noise generation through a number of effects.

(i) Local elastic deformation due to the contact stiffness affects the wheel/rail dynamic interaction. At high frequencies the roughness tends to be absorbed by the contact spring rather than exciting the rail or wheel [2]. For practical changes in contact geometry, however, only small changes in the noise generation occur [3]. This effect is included

*Tel.: +44-23-8059-2510; fax: +44-23-8059-3190.
E-mail address: djt@isvr.soton.ac.uk (D.J. Thompson).

0022-460X/$ - see front matter © 2003 Elsevier Ltd. All rights reserved.
doi:10.1016/S0022-460X(03)00712-0

in the interaction model within the TWINS software [4] and is not considered further in this paper.

(ii) The contact zone between the wheel and the rail exists over an area typically 1 cm in length in the rolling direction. Roughness at wavelengths that are small in comparison with this length does not excite the system as effectively as longer wavelength roughness, an effect known as the 'contact filter'.

(iii) The contact patch is also typically about 1 cm wide and any variations in roughness profile height across the width of the contact patch tend to be averaged out.

(iv) As well as the vertical roughness input, the two-dimensional roughness profile can cause the centre of the contact on the wheel and rail to oscillate from side to side, even in the absence of lateral motion of the wheel relative to the rail. Since the normal load acts effectively at this point, this means that, in addition to the normal load at the *nominal* contact point, an oscillating moment exists. This can also induce vibration and noise [5].

Remington [6] developed an analytical model for the contact filter effect that included both effects (ii) and (iii) above, the latter effect by making an assumption about the degree of correlation across the width of the contact. More recently, a numerical 'distributed point-reacting spring' (DPRS) model has been developed that relies on detailed roughness measurements on a series of parallel lines on the running surface [7]. In this paper, this model is used with a range of measured roughness data to determine the contact filter effect, and these results are compared with the analytical predictions. In order to study the potential for moment excitation, the DPRS model has been extended to allow this effect to be quantified using the measured roughness profiles. The rolling noise prediction model TWINS [4,8,9] has also been extended to allow an estimate of the contribution to the radiated noise to be obtained.

2. Contact filter

2.1. Contact patch

The size of the contact zone depends on the wheel radius and the wheel load, as well as the wheel and rail transverse radii of curvature. It is assumed that the surfaces can be defined by radii of curvature R_w for the wheel, R_r for the rail and R_{wt} for the wheel transverse curvature (negative for concave), as shown in Fig. 1. For such surfaces, the contact patch is elliptical with semi-axis lengths given by

$$a = \sigma_1 \left(\frac{3Pr_e}{2E^*}\right)^{1/3}, \quad b = \sigma_2 \left(\frac{3Pr_e}{2E^*}\right)^{1/3}, \tag{1}$$

where P is the normal load, $E^* = E/(1-\nu^2)$ is the plane strain elastic modulus with E the Young's modulus and ν the Poisson ratio, and r_e is given by

$$\frac{1}{r_e} = \frac{1}{2}\left(\frac{1}{R_w} + \frac{1}{R_{wt}} + \frac{1}{R_r}\right). \tag{2}$$

The two parameters σ_1 and σ_2 in Eq. (1) also depend on R_{ij} and are tabulated, for example, in Ref. [5]. The contact filter reduces the excitation due to roughness at wavelengths that are short in

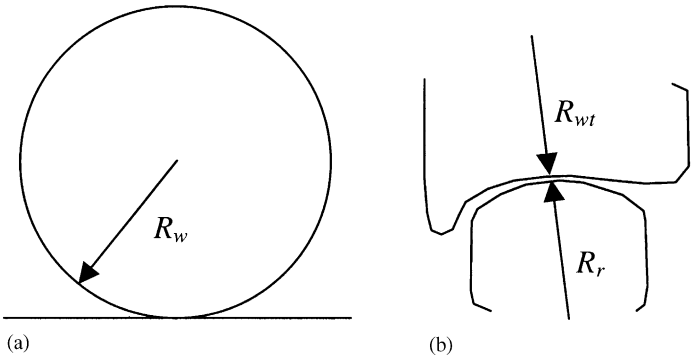

Fig. 1. Wheel and rail radii of curvature at the contact, R_w, R_r and R_{wt}.

comparison with the contact patch length. Two methods of calculating the contact filter are considered.

2.2. Analytical contact filter

An analytical expression for the contact filter was derived by Remington [6]. For a circular contact patch of radius a, the filter transfer function is given by

$$|H(k)|^2 = \frac{4}{\alpha}\frac{1}{(ka)^2}\int_0^{\tan^{-1}\alpha} J_1^2(ka\sec\psi)\,\mathrm{d}\psi, \tag{3}$$

where $k = 2\pi/\lambda$ is the roughness wavenumber in the longitudinal direction, λ being the wavelength, and α is a parameter that describes the degree of correlation between roughness across the width of the contact zone at a given wavenumber. Large values of α imply poor correlation. It is unclear what value of α should be used, so several values were considered.

2.3. DPRS model

The second method considered for deriving the contact filter is numerical. The contact zone between a rigid wheel and rail is approximated by a series of non-linear point-reacting springs [7]. The stiffness behaviour of these springs is chosen with the force proportional to the square root of deflection in order to give the correct overall relationship between force and deflection. Moreover, the radii of curvature of the wheel and rail have to be adapted in order to ensure that the contact area is correct.

In Ref. [7] a high pass filter was introduced, as shown schematically in Fig. 2. It replaces the totally rigid wheel by a mass mounted on a damper. By appropriate choice of the mass this can follow the long wavelength roughness while compressing the (non-linear) contact spring at high frequencies, corresponding to shorter wavelengths. If this filter were not present, the wheel could completely unload or conversely the load could become excessive, leading to an oversized contact patch. The introduction of this filter is a necessary precaution as large amplitudes at very long wavelengths are often present in the roughness data but have no relevance to noise generation.

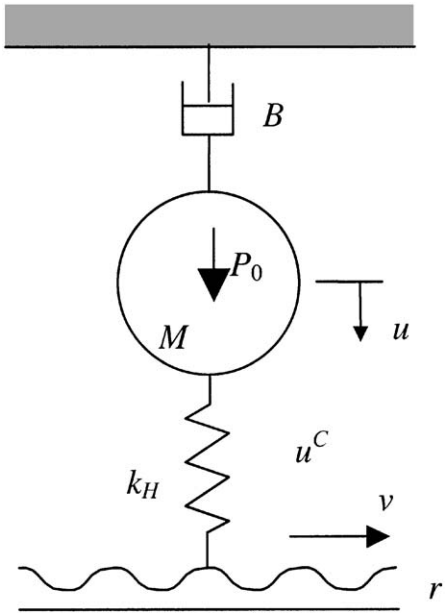

Fig. 2. High-pass filter included in the discrete point reacting spring model. The (non-linear) contact stiffness k_H represents the DPRS model itself.

The motion of the mass satisfies

$$v^2 Mu'' + vBu' = P_0 - P_b(u, r), \tag{4}$$

where u is the displacement of the mass, M, $'$ indicates differentiation with respect to longitudinal distance and B is the damper rate. The force P_b is the total load in the contact spring. It depends on the vertical position of the mass and the roughness profile r at several points around the nominal contact point. The speed v is included to convert time derivatives into spatial derivatives. In the model the mass M is chosen, according to the speed, such that the resonance frequency of the mass on the contact stiffness k_H (implicit in P_b) corresponds to a chosen wavelength of roughness, $\lambda_{res} = 2\pi v(M/k_H)^{1/2}$. The damper rate, B, defined in terms of a loss factor η, $B = \eta k_H \lambda_{res}/2\pi v$, is chosen to prevent the system oscillating too much. The system is solved using a simple time-stepping algorithm to obtain the 'blocked' force P_b; it is strictly only a blocked force for wavelengths shorter than λ_{res}. In Ref. [3] only results for wavelengths shorter than λ_{res} were presented. This has been extended here in the following way.

An instantaneous equivalent roughness r_{eq} can be extracted from the above model using

$$u = u^C - r_{eq}, \tag{5}$$

where u^C is the compression of the (non-linear) contact spring, which can be estimated from the 'blocked' force P_b divided by the nominal (linearized) contact stiffness k_H, provided that $|P_b| \ll P_0$,

$$r_{eq} = u^C - u \approx (P_b/k_H) - u. \tag{6}$$

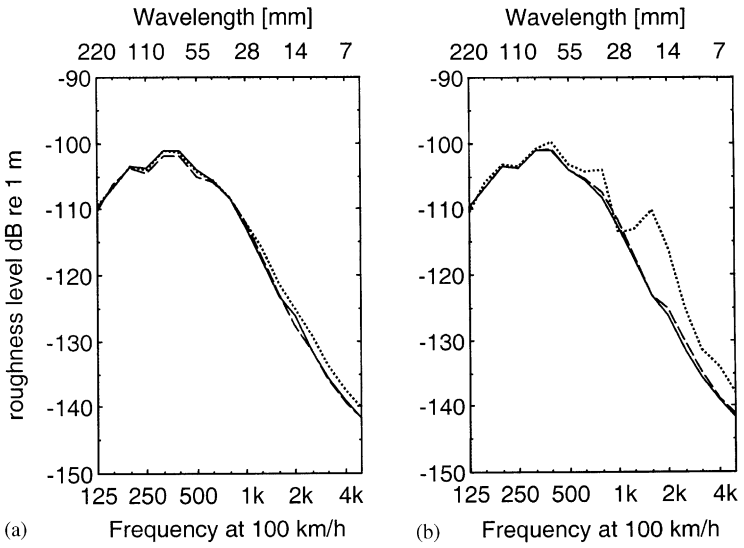

Fig. 3. Equivalent roughness obtained from roughness of cast-iron block braked wheel with transverse radius −330 mm and rail radius of curvature 300 mm. (a) different resonant wavelengths (for $\eta = 1$), —— $\lambda_{res} = 30$ mm, – – – $\lambda_{res} = 100$ mm, ····· $\lambda_{res} = 10$ mm; (b) different loss factors (for $\lambda_{res} = 30$ mm), —— $\eta = 1$,– – – $\eta = 0.5$, ····· $\eta = 0.1$.

This result should apply irrespective of the choice of 'resonant wavelength', provided that the non-linearity of the contact spring does not become too marked. Fig. 3 shows example results for different values of λ_{res} and η.

It can be seen that using different values of λ_{res} has only a very small effect on the result for r_{eq}. The reduction in level at the peak for $\lambda_{res} = 100$ mm is due to the blocked force having a larger amplitude and therefore inducing greater non-linearity in this case. Otherwise the correction according to Eq. (6) eliminates the effect of the high pass filter. The results for $\eta = 0.5$ or 1 are equivalent but those for $\eta = 0.1$ show significant contamination at high frequency, due to bouncing of the wheel at the resonance frequency leading to loss of contact.

2.4. Measured roughness data

For use with the DPRS model, roughness measured on many parallel lines on the wheel or rail is required. Here, six sets of measured roughness data have been used, from wheels with cast-iron block brakes, sinter block brakes and disc brakes [3]. These roughness measurements were made on 25 lines at 2 mm intervals across the width of the running surface, and sampled at 0.5 mm intervals around the perimeter. In order to evaluate the contact filter, the results from the DPRS model are compared with the average of the roughness spectra from the four or five measurement lines passing through the contact zone. No account has been taken here of the need to fill pits or deal with spikes [10] as the measurements are relatively free of such features.

Frequency spectra were obtained from both the results from the DPRS model and the unfiltered roughness in the same way. Any linear trend is first removed and the mean is set to zero. Then a single Fourier transform is calculated without windowing, and these narrow-band results

Table 1
Wheel radii and wheel loads considered for contact filter calculations

Wheel radius (mm)	Wheel loads (kN)	Contact stiffness (GN/m)	Contact patch semi-length, a (mm)	Contact patch semi-width, b (mm)
460	25	0.900	4.53	3.42
	50	1.144	5.69	4.28
	100	1.426	7.20	5.40
327	50	1.078	4.81	4.54
180	50	0.979	3.56	4.99

are integrated into one-third octave bands. In all cases results are presented in terms of frequency at a speed of 100 km/h (27.8 m/s). The rail radius of curvature was set to 300 mm, the value applying to a new rail profile. The wheel transverse profile was assumed to be coned (i.e., flat). Various values of wheel radius and load were considered, as listed in Table 1. The corresponding contact patch dimensions and linearized contact stiffness are also listed.

2.5. Contact filter results

The average roughness of two of the wheels used is shown in Fig. 4. These spectra were determined using approximately one revolution of the wheel. The disc-braked wheel contained a 'flat' near the start of the measured data, which was removed by analysing slightly less than one revolution. It can be seen that the block-braked wheel has a broad peak at around 400 Hz (70 mm wavelength). The disc-braked wheel has a much lower roughness at low frequencies, but above about 2.5 kHz its roughness is higher than that of the block-braked wheel.

The filtered results from the DPRS model are also shown. Results are given for 460 and 180 mm radius wheels, in each case for a 50 kN preload. Up to about 800 Hz (35 mm) the filtered and unfiltered roughnesses are similar. At higher frequencies, the contact filter reduces the effective roughness due to averaging over the length of the contact patch. The smaller wheel has a shorter contact patch ($a = 3.6$ mm instead of 5.7 mm, see Table 1), by a factor of 1.6. It would therefore be expected that the contact filter effect would take effect at frequencies about two one-third octaves higher for the smaller wheel. This is approximately the case.

The contact filter results obtained from the two methods are compared in Fig. 5 for a 460 mm radius wheel with 50 kN preload. The results from the DPRS model are the differences between the filtered and unfiltered results in Fig. 4. The analytical model of Eq. (3) applies to a circular contact patch whereas those here are elliptical (see Table 1). For simplicity the model has been used here with the semi-axis length in the rolling direction a in Eq. (3). The analytical model was used to calculate results at four frequency points in each one-third octave band before conversion to one-third octave spectra. From Fig. 5 it can be seen that the analytical model gives similar results to the numerical DPRS method provided that a value of α between about 1 and 3 is used. The filter effects from the DPRS model using both the tread-braked and disc-braked wheel roughnesses are similar.

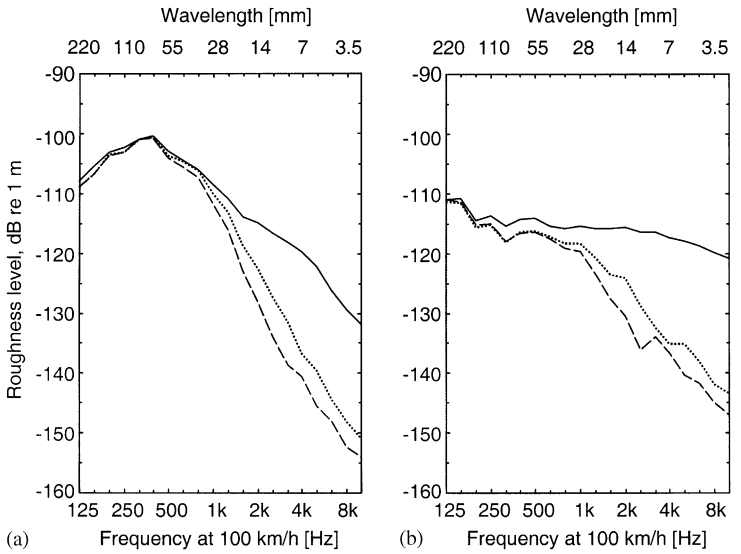

Fig. 4. Comparison of average roughness over 5 or 4 lines across contact patch with results from DPRS model for two wheel radii and 50 kN wheel load. (a) Cast-iron block tread-braked wheel roughness; (b) disc-braked wheel roughness. —— unfiltered, – – – 460 mm radius wheel, ····· 180 mm radius wheel.

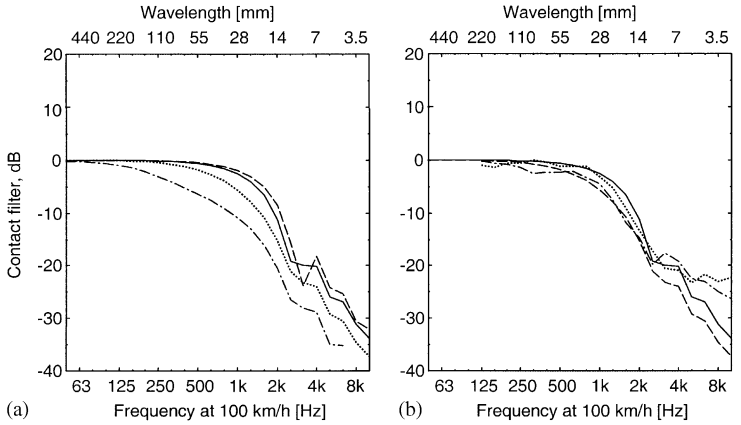

Fig. 5. Contact filter due to 460 mm wheel radius, 50 kN load. (a) Analytical model: —— $\alpha = 1$, – – – $\alpha = 0.1$, ····· $\alpha = 3$, – · – · $\alpha = 10$; (b) —— analytical, $\alpha = 1$, – – – analytical, $\alpha = 3$, ····· numerical (DPRS), cast-iron block-braked wheel roughness, – · – · numerical (DPRS), disc-braked wheel roughness.

At high frequencies the result from the analytical model falls at about 30 dB per decade. Above about 4 kHz (wavelengths smaller than 7 mm) the filter effect of the DPRS model is less than that calculated by the analytical method, falling more slowly with increasing frequency. This is believed to be due to the fact that the DPRS model takes account of the variation of the normal load across the contact zone. Both models show dips at wavelengths of around $2a$ (2.5 kHz) and a (5 kHz).

Fig. 6(a) compares the contact filter effect calculated using the DPRS model for all six sets of wheel roughness data. The results are very similar. A mean line is also shown, which is the average

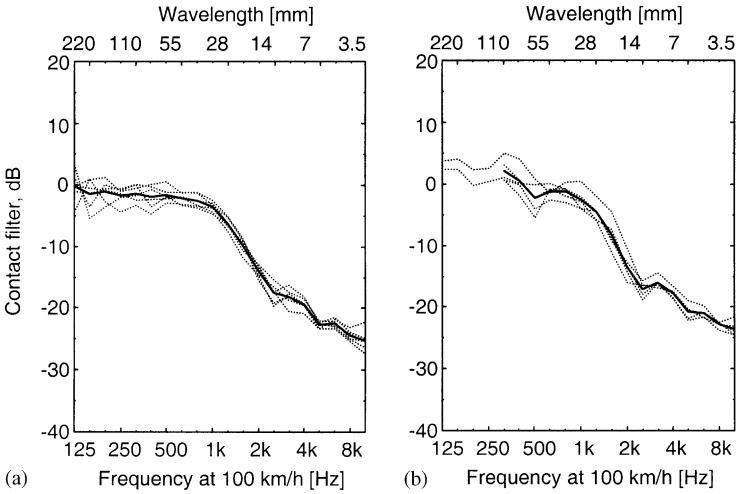

Fig. 6. Contact filter from DPRS model for 460 mm wheel radius, 50 kN load. (a) Three cast-iron block-braked wheels, one disc-braked wheel and two sinter block-braked wheels. —— mean of six wheels; (b) results from Ref. [9]: one cast-iron block-braked wheel, one disc-braked wheel and three rails. —— mean of five results.

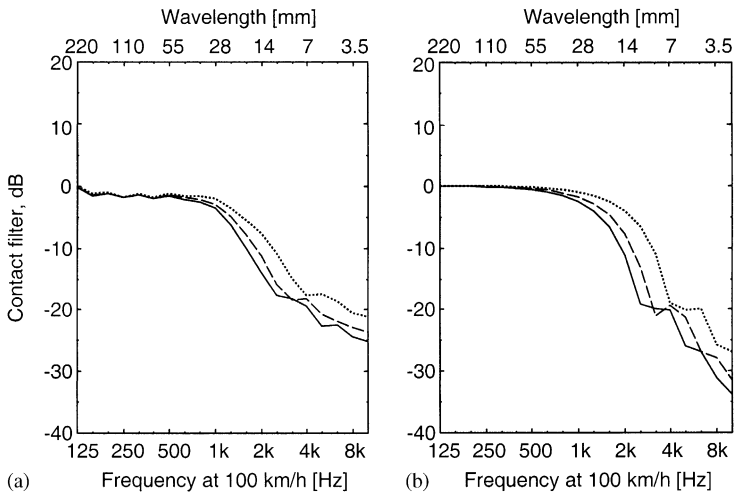

Fig. 7. Contact filter due to various wheel radii, 50 kN load. (a) Average result from DPRS model; (b) analytical model. —— 460 mm radius wheel, – – – 327 mm radius wheel, ····· 180 mm radius wheel.

of the six contact filter results. In the remainder of this section this mean over all six sets of wheel roughness is plotted for various radii and wheel loads. Fig. 6(b) shows equivalent results for the roughness measurements from Ref. [9] for two wheels and three rails. A similar mean filter effect is found as in Fig. 6(a). A similar comparison was given in Ref. [10] but this used an earlier version of the DPRS program that has since been discovered to contain minor errors. The present results are closer to those in Fig. 6(a) and contain much less scatter than those in Ref. [10].

In Fig. 7 the effect of wheel radius is shown. In both sets of results the whole contact filter curve is effectively shifted to the right as the contact patch length is reduced. The filter rolls off at a

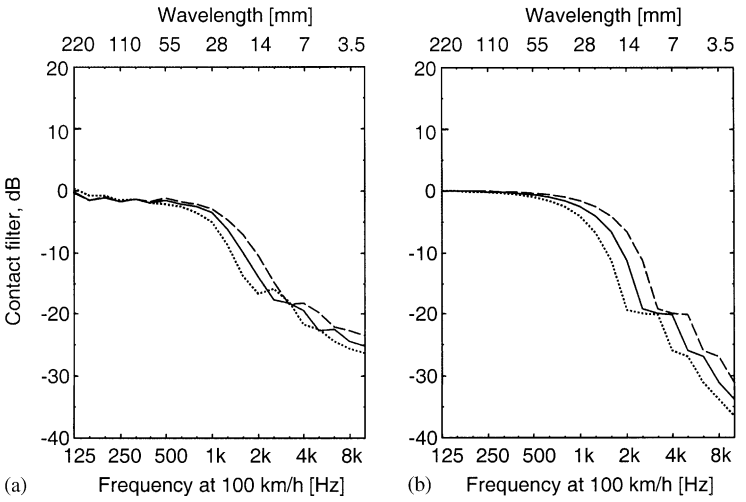

Fig. 8. Contact filter due to various wheel loads, 460 mm radius. (a) Average result from DPRS model; (b) analytical model. —— 50 kN, – – – 25 kN, ····· 100 kN.

wavelength λ which is related to the contact patch length; it reaches a minimum when $\lambda \approx 2a$. From the contact patch dimensions in Table 1, these wavelengths correspond to frequencies of 2440, 2890 and 3900 Hz. As in Fig. 5, the two methods agree at low frequencies but diverge at high frequencies. This occurs for wavelengths smaller than about $1.25a$, i.e., at about 7 mm for the 460 mm radius wheel, and correspondingly shorter than this for the smaller wheels.

The effect of the wheel load is illustrated in Fig. 8. Again, the contact patch length determines the wavelength at which the filter rolls off; here $\lambda = 2a$ at 1930, 2440 and 3070 Hz. Once more the two methods diverge for wavelengths shorter than about $1.25a$.

3. Moment excitation

3.1. Model for moment excitation

For a given pair of wheel and rail transverse profiles, the nominal contact point depends on the lateral position of the wheelset on the track. This is the point at which contact would initially occur if the wheel were lowered onto the rail. An example is shown in Fig. 9, where the lines joining the two profiles indicate the point of contact on the two bodies for various lateral wheelset positions, y. From this, it appears that the nominal contact position can jump quite large distances across the running surfaces for small changes in wheelset position. This phenomenon occurs at two lateral wheelset positions that are, in fact, the stable positions at which the wheelset is most likely to run [3].

As the wheel runs along the rail, the transverse profiles can change slightly due to the addition of roughness. Thus it is possible, for a constant wheelset position, for the contact position to fluctuate laterally across the railhead and wheel tread. In Ref. [5] (see also Ref. [2]) it was shown that this can be conceived as a moment excitation of the system that can be an additional source

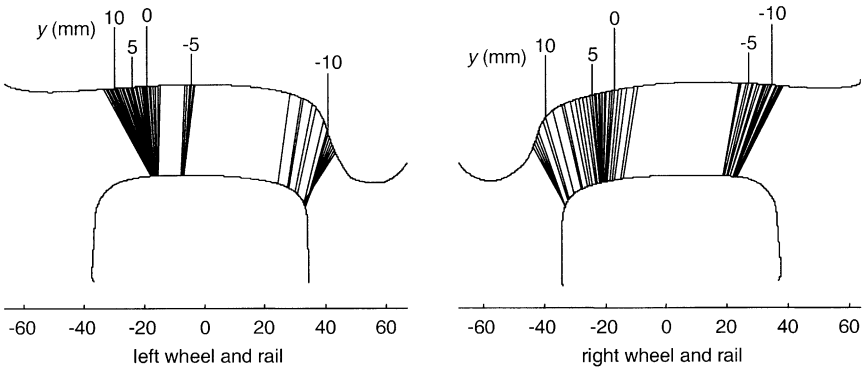

Fig. 9. Transverse profile of a worn wheel profile (sinter block tread-braked) in combination with a UIC54 rail.

of excitation of the wheel/rail system. The normal load at the contact point can be expressed as the sum of the static load P_0 and the dynamic load, P, $P_{tot} = P_0 + P$. In the TWINS calculation model only the dynamic component excites the vertical vibration. If the centre of the contact patch moves laterally a distance ε relative to the *nominal* contact position, the normal load induces a moment $M = \varepsilon(P_0 + P) \approx \varepsilon P_0$ about the rolling direction with respect to the original position. If the distance ε varies, the corresponding variation in this moment excites the wheel/rail system. Its magnitude is greatest for large static wheel loads, P_0. Although this model was proposed in Ref. [5], insufficient measurement data were available at that time to quantify its effect. The data required are roughness measurements along many parallel lines through the contact zone and wheel and rail transverse profiles. Data of this form were measured within a recent European project, and have been used in Section 2.5 above; see also Ref. [3].

Using the DPRS model with the measurements of roughness described above, the moment about the rolling direction has been derived at each position along the track. This has been Fourier transformed and then converted to a one-third octave band spectrum. The model for the excitation of the wheel/rail system by this moment is described in more detail in Ref. [5]. Unfortunately, the DPRS model cannot currently be used directly in conjunction with measured transverse profiles. This is due to the fact that the surfaces have to be defined in the model by fixed radii of curvature. This is necessary to allow the transformation to equivalent radii for scaling the contact patch dimensions. In the following, therefore, various fixed values of wheel transverse radius are considered with a rail radius of 300 mm. Of course, the actual wheels considered had one particular transverse profile but as this was not circular it cannot be analyzed directly. Instead a range of values is considered in order to study the effect of this parameter.

3.2. Results

Average roughness levels and moment levels have been determined based on the measurement data for each of seven wheels. Fig. 10 shows the results for the roughness from a cast-iron block braked wheel assuming different transverse profile radii of the wheel. This clearly shows that the moment excitation increases considerably as the contact becomes more conforming. Fig. 11 shows the calculated noise levels due to roughness and moment excitation, for the same wheel as in the

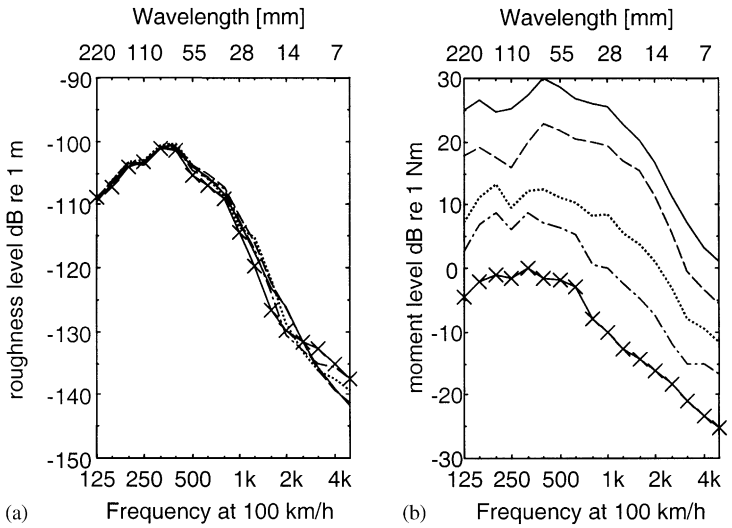

Fig. 10. Equivalent roughness level and moment level from measured roughness and different transverse radii. —— $R_{wt} = -330$ mm, – – – $R_{wt} = -400$ mm, ····· coned wheel, – · – · $R_{wt} = +200$ mm, ×—× $R_{wt} = +60$ mm.

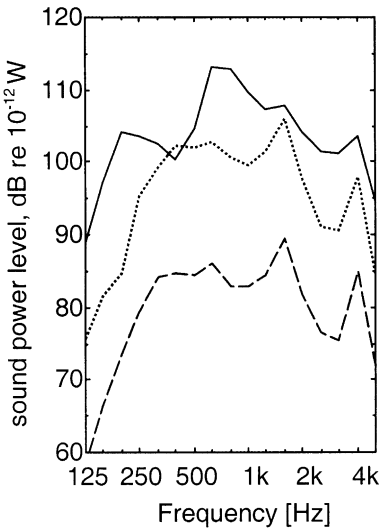

Fig. 11. Sound power level due to roughness and moment excitation, for a cast-iron block-braked wheel at 100 km/h. —— due to roughness, 118.1 dB(A), – – – due to moment for coned wheel, 94.8 dB(A), ····· due to moment for conforming wheel ($R_{wt} = -330$ mm), 111.2 dB(A).

figures above. In the case of the coned wheel, the moment excitation is not significant. The conforming profile increases the noise due to moment excitation by 16 dB so that it is only 7 dB(A) less than that due to the conventional roughness excitation. The results in Figs. 10 and 11 are all for a wheel load of 50 kN. Fig. 12 shows that as the wheel load is increased, the moment excitation increases, particularly for frequencies up to about 1 kHz.

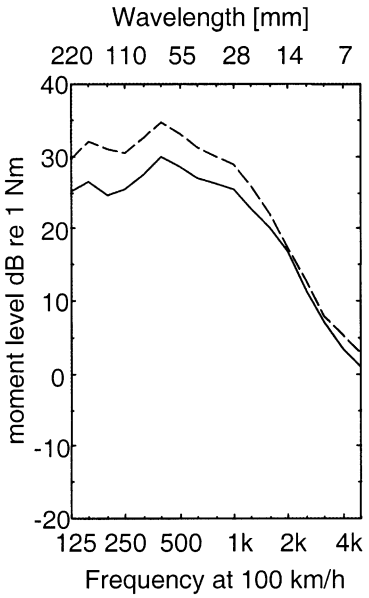

Fig. 12. Moment level for $R_{wt} = -330$ mm. —— 50 kN wheel load, – – – 100 kN.

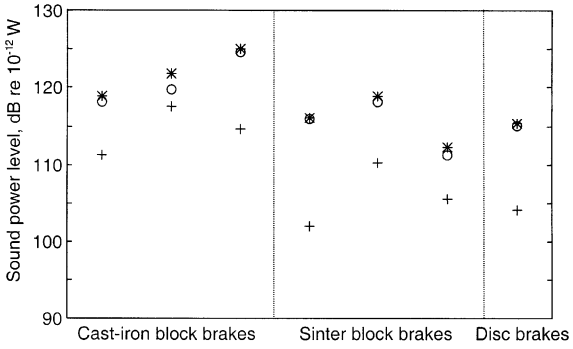

Fig. 13. Sound power level due to roughness and moment excitation from roughness of seven different wheels for a wheel transverse radius of −330 mm. ∗ total, ○ due to roughness, + due to moment.

Sets of roughness data for the other measured wheels result in moment excitation noise levels that vary between 2 and 15 dB(A) below that of the roughness excitation, as shown in Fig. 13. Therefore, it may be concluded that moment excitation can be a significant additional mechanism for conforming profiles. In extreme cases it may be comparable to conventional roughness excitation. Further work is required, however, to incorporate the actual transverse profiles into the DPRS calculation.

4. Conclusions

A distributed point-reacting spring (DPRS) model has been used with measured roughness data to determine the contact filter effect. Comparing this result with analytical predictions, it is

found that the analytical model gives an attenuation that is too large at high frequencies (wavelengths shorter than about $1.25a$, which is 7 mm for a typical wheel radius of 460 mm). At wavelengths longer than the contact patch length, using a value of the correlation parameter α between 1 and 3 good agreement is found between the results of the analytical and numerical models.

Additionally, moment excitation due to variations in contact patch location has been analyzed. In extreme cases of conforming wheels and rails, the noise level due to this excitation mechanism is comparable to that of roughness excitation.

Acknowledgements

Some of the work reported here was performed within the EU project STAIRRS, contract number 1999RD.10442, project number B99/99/S12.107978-B66131122 and the EU Brite Euram project Silent Freight, project number BE95-1238, contract number BRPR-CT95-0047, both co-ordinated by ERRI. The wheel roughness measurements were carried out by TNO-TPD and profiles were measured by NSTO (now AEA Technology Rail BV).

References

[1] D.J. Thompson, C.J.C. Jones, A review of the modelling of wheel/rail noise generation, *Journal of Sound and Vibration* 231 (2000) 519–536.
[2] D.J. Thompson, Wheel/rail noise generation, Part IV: contact zone and results, *Journal of Sound and Vibration* 161 (1993) 447–466.
[3] D.J. Thompson, P.J. Remington, The effects of transverse profile on the excitation of wheel/noise, *Journal of Sound and Vibration* 231 (2000) 537–548.
[4] D.J. Thompson, M.H.A. Janssens, TWINS: Track-wheel interaction noise software. Theoretical manual, version 2.4, TNO report TPD-HAG-RPT-93-0214, TNO Institute of Applied Physics, 1997.
[5] D.J. Thompson, Wheel/Rail Noise—Theoretical Modelling of the Generation of Vibrations, Ph.D. Thesis, University of Southampton, 1990.
[6] P.J. Remington, Wheel/rail noise—IV: rolling noise, *Journal of Sound and Vibration* 46 (1975) 419–436.
[7] P.J. Remington, J. Webb, Estimation of wheel/rail interaction forces in the contact area due to roughness, *Journal of Sound and Vibration* 193 (1996) 83–102.
[8] D.J. Thompson, B. Hemsworth, N. Vincent, Experimental validation of the TWINS prediction program for rolling noise—1: description of the model and method, *Journal of Sound and Vibration* 193 (1996) 123–135.
[9] D.J. Thompson, P. Fodiman, H. Mahé, Experimental validation of the TWINS prediction program for rolling noise—2: results, *Journal of Sound and Vibration* 193 (1996) 137–147.
[10] D.J. Thompson, On the relationship between wheel and rail surface roughness and rolling noise, *Journal of Sound and Vibration* 193 (1996) 149–160.